JACS
JOURNAL OF THE AMERICAN CHEMICAL SOCIETY
Article
pubs.acs.org/JACS

Direct STM Elucidation of the Effects of Atomic-Level Structure on Pt(111) Electrodes for Dissolved CO Oxidation

Junji Inukai,*[,†] Donald A. Tryk,[†] Takahiro Abe,[‡] Mitsuru Wakisaka,[†] Hiroyuki Uchida,*[,†,§] and Masahiro Watanabe*[,†]

[†]Fuel Cell Nanomaterials Center, University of Yamanashi, 6-43 Miyamae-cho, Kofu, 400-0021, Japan
[‡]Interdisciplinary Graduate School of Medicine and Engineering, University of Yamanashi, 4-3 Takeda, Kofu 400-8511, Japan
[§]Clean Energy Research Center, University of Yamanashi, 4 Takeda, Kofu 400-8510, Japan

Supporting Information

ABSTRACT: We sought to establish a new standard for direct comparison of electrocatalytic activity with surface structure using in situ scanning tunneling microscopy (STM) by examining the electrooxidation of CO in a CO-saturated solution on Pt(111) electrodes with steps, with combined electrochemical measurements, in situ STM, and density functional theory (DFT). On pristine Pt(111) surfaces with initially disordered (111) steps, CO oxidation commences at least 0.5 V lower than that for the main oxidation peak at ca. 0.8−1.0 V vs the reversible hydrogen electrode in aqueous perchloric acid solution. As the potential was cycled between 0.07 and 0.95 V, the CO oxidation activity gradually decreased until only the main oxidation peak remained. In situ STM showed that the steps became perfectly straight. A plausible reason for the preference for (111) steps in the presence of CO is suggested by DFT calculations. In contrast, on a pristine Pt(111) surface with rather straight (100) steps, the low-potential CO oxidation activity was less than that for the pristine, uncycled (111) steps. As the potential was cycled, the activity also decreased greatly. Interestingly, after cycling, in situ STM showed that (111) microsteps were introduced at the (100) steps. Thus, potential cycling in the presence of dissolved CO highly favors formation of (111) steps. The CO oxidation activity in the low-potential region decreased in the following order: disordered (111) steps > straight (100) steps > (100) steps with local (111) microsteps ≈ straight (111) steps.

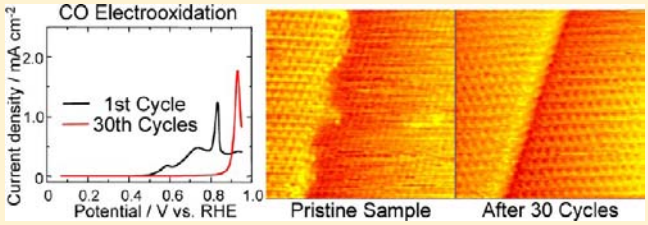

1. INTRODUCTION

Surface structure−activity relationships are crucial for study of surface reactions of all types, including those that are important in catalysis,[1−9] electrochemistry and electrocatalysis,[10−22] and metal oxide surface chemistry, including photocatalysis.[23−31] Scanning probe microscopies, particularly scanning tunneling microscopy (STM), have already produced exciting results in these areas, even to the point of showing chemical processes at the atomic or molecular level on surfaces in real time (see, for example, STM videos from the Besenbacher group).[32] However, to achieve this feat, it is usually necessary to employ very special experimental conditions, e.g., low pressure and/or low temperature. For a number of years, it has been possible to achieve atomic resolution in STM images in liquid electrolytes at ambient temperature and pressure, with potential control, so that ordered adsorbate layers can be observed.[11−22] It has also been possible to observe electrode surfaces even as electrochemical reactions are occurring, for example, etching[10,14] and electrodeposition and reconstruction,[33−38] i.e., processes involving displacement of many atoms. The Itaya group reported in situ, real-time etching processes on semiconductor[10,39] and metal[39−42] electrodes elucidating the reaction mechanism on the atomic scale. Some examples of real-time videos, including metal electrodeposition, have been presented by the Magnussen group.[43] Also, it has been possible to observe electrodes such as Pt single crystals simultaneously with a quasi-steady-state molecular-level reaction such as oxidation of dissolved carbon monoxide.[44−46] In the present work, two of these strategies have been used, first, to examine, in situ, progressive changes in step edge structures on Pt(111) and related stepped single crystals during potential cycling and, second, to observe the effects of such structures on the CO adsorption configuration, both short and long range, and on the macroscopic-level current for CO oxidation. Thus, we are able to establish extremely direct relationships between the prevailing surface structure and the relative magnitude of the anodic oxidation current. Of course, the actual electrochemical reaction occurs at such a rapid rate that no changes can be observed in the STM images.

There is already a vast body of literature on the electrochemical oxidation of CO, particularly on the platinum surface.[47−49] Specific examples include the work of the research groups of Cuesta,[50−54] Feliu,[55−71] Koper,[57,65,67,72−75] Korze-

Received: October 19, 2012
Published: January 7, 2013

   dx.doi.org/10.1021/ja309886p | J. Am. Chem. Soc. 2013, 135, 1476−1490

niewski,[76,77] Markovic,[78−87] Stimming,[88−93] Vielstich,[87,95] and Wieckowski,[55,68,96−101] as well as studies involving vibrational spectroscopy, for example, by Ito,[102] Osawa,[103−105] and our group.[106−111] Many papers have been devoted to oxidation of an adsorbed monolayer of CO, often referred to as CO stripping. This reaction usually occurs at a relatively high potential, in the 0.7−1.0 V range vs the reversible hydrogen electrode (RHE), within a narrow potential range, which reflects the fact that it is occurring far from the equilibrium potential for the reaction, −0.104 V vs RHE,[105,114] due partly to CO molecules forming a tight, protective surface layer, which rather effectively blocks access of water molecules to the platinum surface.

However, intriguingly, current can often be observed to flow in the lower potential region, from 0.3 to 0.5 V vs RHE, depending both on the characteristics of the Pt surface and also to some extent on the potential at which CO was initially adsorbed. This current has been variously referred to as "prepeak", "prewave", "preoxidation", or "preignition" current. The origins of this current have been controversial, and several different explanations have been advanced. It has been considered by some researchers that the prepeak is due principally to higher coverages of CO that can exist at lower adsorption potentials, for example, close to zero on the RHE potential scale.[96,127] With high coverages, there could exist more weakly adsorbed CO molecules, which could be oxidized more easily, i.e., at lower potentials, which is a reasonable idea. One problem with this explanation, however, is that the (2 × 2)−3CO structure with coverage 0.75 is rather stable from low potentials (ca. 0.05 V) all the way up to 0.55 V on Pt(111) with few defects,[59] whereas the low-potential oxidation can begin at ca. 0.35−0.4 V. In contrast, it has also been considered that the prepeak is due to CO oxidation at steps or other defects, at which OH is known to adsorb preferentially,[50,54,61,65,67] although the onset potential (ca.0.35−0.4 V) is so low that OH cannot be expected to form, even at steps.[71] If there is CO dissolved in the electrolyte solution, the current can flow steadily, since CO is being supplied continuously from the solution, in contrast to the situation in which there is only a monolayer of CO present on the surface.

This phenomenon of high catalytic activity at low potentials on pure, unalloyed platinum is of great interest, because it implies that there might be a rather simple explanation, since there are no complications that arise when dealing with alloys, and it demonstrates that pure Pt is capable of sustained catalytic activity, without becoming poisoned. CO poisoning is a significant problem for hydrogen anodes in polymer electrolyte fuel cells that are fed with natural gas-derived hydrogen.[112] If the details of this effect could be understood, it would have a significant impact on the design of CO-tolerant hydrogen oxidation reaction (HOR) electrocatalysts.

Also of great interest is the observation that sweeping the potential over a wide range, e.g., 0.1−1.0 V vs RHE in the presence of dissolved CO, serves to deactivate the surface toward CO oxidation in the prepeak region, as pointed out by Wieckowski et al.[94] and later studied intensively by Markovic and co-workers,[77,87] Stimming and co-workers,[89,91] and Arenz and co-workers.[115] Recently, Strmcnik et al., using ex situ STM, presented results that have provided insight into this process and found that the presence of Pt islands and other low coordination structures on the Pt(111) surface is associated with high activity for CO oxidation at low potentials.[81] They found that, during the potential cycling process, these islands were removed. Thus, the authors proposed that the steps associated with islands, particularly at the nanometer level, are important catalytic sites, due to their low coordination number (CN).

Very recently, the controversy has centered upon in situ infrared spectroscopic results from three laboratories, including our own.[92,103,111] Three somewhat different explanations of the prepeak activity have emerged, based on the variations in the surface coverages of several different types of adsorbed CO species, including bridging and atop CO molecules on terraces vs those at steps or other defects. Our work has suggested that atop CO on terraces can diffuse toward steps, forming bridging CO, which might be oxidized easily.[111]

In an effort to shed light on this situation from a different direction, we have recently been examining this phenomenon further with atomic-resolution in situ STM, under conditions in which the overall CO oxidation current can be measured in an electrochemical cell. As reported herein, we found that the various types of possible step structures can be understood in more detail. In fact, we find that the atomic-level structure of the step itself is important, so that some types of step structures are highly active, while others are nearly inactive for CO oxidation at low potentials.

The results are somewhat inconsistent with experimental[147,148] and theoretical[111] gas-phase results for the CO + O (or O_2) reaction, which have concluded either that (111) steps are the most active[147,148] or that the CO oxidation activity is most active for the flat (111) terrace and decreases with decreasing CN for Pt.[111] Our results, in agreement with those of Markovic and co-workers,[81] suggest that the activity increases in the order terraces < steps < kinks < step-adatoms (single adatoms at steps),[117] i.e., increasing activity with decreasing CN. Recent in situ STM results of Rudnev and Wandlowski for CO oxidation on Pt(100) also support kinks and steps as having higher activity.[46] The exact atomic- and molecular-level details are of great interest. Here, using atomic-resolution in situ STM and macroscopic cyclic voltammetric measurements *on the same surface under identical conditions* we are able to establish extremely clear relationships between the surface structure and the electrocatalytic activity. By maintaining all conditions exactly the same, we are thus able to focus on the structural aspect alone without the influence of other complications such as adsorption potential or the characteristics of the anion.

While the exact mechanistic details can only be hinted at here, we laid a firm foundation for further mechanistic studies, including theoretical calculations. Although we cannot specify the exact catalytic sites at present, we can greatly narrow down the search for such sites. We can conclude with certainty that disordered (111) steps, which include low CN Pt atoms, have the highest catalytic activity and that one of the primary reasons is that the ordering of the CO adlayer, which is superbly uniform and protective, *even across a perfect (111) step*, is disrupted at such disordered steps, allowing water to participate in CO oxidation at low potentials.

One of the most striking findings of the present work is that potential cycling in the presence of CO tends to strongly favor transformation of steps to maximize the occurrence of (111) steps, so that, for example, initially disordered (111) steps become perfectly straight and initially straight (100) steps become zigzagged with (111) microsteps. Both become highly inert, again due to the superb ordering of the CO adlayer across the step. We are able to offer a tentative explanation of this

dx.doi.org/10.1021/ja309886p | J. Am. Chem. Soc. 2013, 135, 1476−1490

unusual phenomenon, based on high-accuracy DFT calculations. Thus, we are now able to provide deeper insight into both the restructuring of steps on Pt during potential cycling in the presence of CO and the possible reasons why the coordination number might be important in electrocatalysis, particularly in providing catalytic sites at which CO can be continuously oxidized at low potentials. This new, atomic-level insight, with a direct link between surface structure and electrocatalytic activity, can provide a significant step forward in guiding the design of new, more active catalysts and electrocatalysts for CO oxidation and CO-tolerant hydrogen oxidation. Even more importantly, we believe that this work helps to establish a new standard for direct comparison of electrocatalytic activity and surface structure.

2. EXPERIMENTAL SECTION

2.1. Electrochemical and STM Measurements. Single-crystal beads of Pt, approximately 3 mm in diameter, were made by crystallization of a molten ball formed at the ends of Pt wires in a hydrogen/oxygen flame.[14,44,45,56] A laser-beam reflection method was employed to determine the orientation of the single-crystal bead to expose the (111) plane, which was then mechanically polished with successively finer grade diamond pastes down to 0.25 μm with an accuracy of <0.2°. For Pt(10 10 9) and (20 19 19) planes, X-ray diffraction was employed to determine those planes prior to mechanical polishing, as reported previously.[118] All of the samples were treated in a hydrogen/oxygen flame for 2 h to eliminate surface damage caused by mechanical polishing. Each sample was placed in an infrared image furnace filled with hydrogen,[45] heated up to 1450 K, and gradually cooled down to 473 K, at which the gas was exchanged to Ar. The sample was taken out and placed in ultrapure water (Milli-Q) saturated with CO to protect the surface from contamination. The Pt electrode was carefully and immediately transferred into an electrochemical cell filled with a 0.1 M $HClO_4$ (ultrapure grade, Kanto Chemical) solution. Electrochemical measurements were carried out at 293 K using a potentiostat with the hanging meniscus method in a three-compartment electrochemical cell. In situ STM measurements with a tungsten tip etched in 1 M KOH were carried out using a Nanoscope-E (Veeco) under an atmosphere of high-purity N_2 or CO. To minimize residual faradaic currents, the tips were coated with transparent nail polish. STM images were recorded in the constant-current mode. A reversible hydrogen electrode (RHE) was used as a reference to control the electrode potential. The same Pt(111), (10 10 9), and (20 19 19) samples were used for both electrochemical and STM measurements. Sample preparation and electrochemical/STM measurements were all carried out in a clean room.

2.2. DFT Calculations. Periodic boundary condition DFT calculations were carried out with the DMol^3 package (versions 4.3 and 6.0, Accelrys, Inc.).[120,121] We first optimized the geometries of the Pt(322) surface, which has (100) steps, and the Pt(553) surface, which has (111) steps, with various coverages and site occupancies of CO close to the step. Both slabs have terraces that are five atoms wide, with thicknesses of three layers at both terraces and steps. In addition, several other surfaces with (111) steps were examined, including Pt(422) (4-row terraces), Pt(664) (6-row terraces), and Pt(443) (8-row terraces), and several others with (100) steps, Pt (866) (7-row terraces) and Pt(10 8 8) (9-row terraces). These geometry optimizations were carried out in the density functional semicore pseudopotential (DSPP) mode,[118] and then the energies of the optimized structures were calculated in the all-electron, scalar relativistic mode. In both cases, the functional used was GGA-PBE[123] and the basis set was double numerical plus polarization (DNP), which is comparable to Gaussian double-ζ plus polarization. Electron smearing (0.005 Ha) was applied to enhance the SCF convergence, and the total binding energies extrapolated to absolute zero electron temperature were used. An orbital cutoff of 5.0 Å was used. The average CO adsorption energies per CO molecule were calculated by subtracting the total binding energies of the appropriate number of gas-phase CO molecules per unit cell plus that of the bare unit cell Pt slab from that of the CO-adsorbed Pt slab and then dividing by the number of CO molecules, in the usual fashion. Procedures used are similar to those described by Orita and co-workers.[124,126]

3. RESULTS AND DISCUSSION

3.1. Electrochemical Measurements on Pt(111) with (111) Steps. Figure 1 shows the results of the cyclic

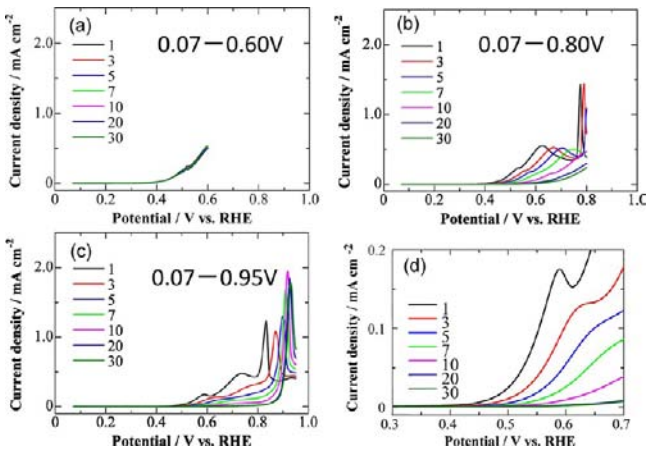

Figure 1. CVs on Pt(111) for CO electrooxidation in a 0.1 M $HClO_4$ solution saturated with CO at 50 mV s^{-1} between 0.07 and 0.6 (a), 0.8 (b), and 0.95 V (c). (d) Onsets for oxidation. Only anodic scans are shown.

voltammograms (CVs) on Pt(111) obtained in a 0.1 M $HClO_4$ solution saturated with CO. The potential was swept repetitively from 0.07 to 0.60 (Figure 1a), 0.07 to 0.80 (Figure 1b), or 0.07 to 0.95 V (Figure 1c) at a scan rate of 50 mV s^{-1}. Only the positive scans are shown in the figures. Potential sweeps were continued for 30 cycles. In Figure 1a, the CO oxidation current starts at 0.4 V and at the highest potential of 0.6 V the current density is seen to be 0.6 mA cm^{-2}. No changes were seen in the CVs during the cycling in this potential range. In Figure 1b, the current, clearly seen to be due to CO oxidation, initially started at 0.4 V. A broad anodic oxidation feature, often termed a "prepeak" but referred to more properly as "low-potential CO oxidation current", at about 0.7 V was seen, followed by a sharp spike at around 0.8 V, known as the main peak for CO oxidation, or "ignition", due to its sudden onset and completion.[127,128] As the number of potential cycles increased, the onset potential moved in the positive direction, the prepeak gradually decreased in intensity, and the main peak shifted to higher potentials (discussed further in Section 3.4). These phenomena are similar to those reported by the Markovic group on both Pt nanoparticles[87] and single-crystal surfaces.[81] By carefully changing the upper limit of the potential sweep it was revealed that the decreasing magnitude of the prepeak is associated with the increasing magnitude of the main peak. When the upper potential limit was increased to 0.95 V, the CO oxidation current at the prepeak decreased faster. Figure 1d is a blow up of the lower potential range in Figure 1c. After 30 cycles, practically no current was seen prior to the main peak.

In Figure 2a, the anodic current profiles of the 1st and 30th cycles are depicted, which were taken from Figure 1c. Before potential cycling, the oxidation started at 0.4 V and a spike, i.e.,

dx.doi.org/10.1021/ja309886p | J. Am. Chem. Soc. 2013, 135, 1476−1490

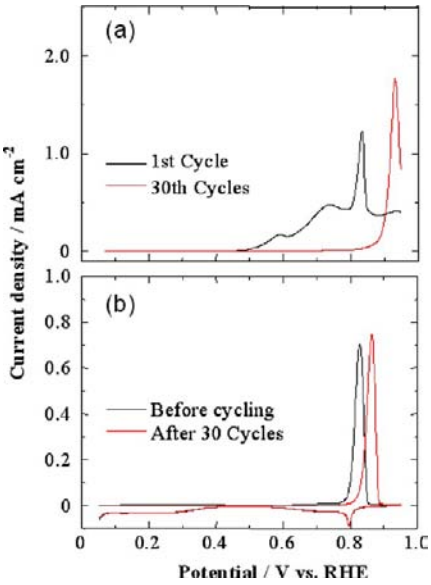

Figure 2. (a) CVs on Pt(111) in a 0.1 M $HClO_4$ solution saturated with CO at 50 mV s^{-1} between 0.07 and 0.95 V for the 1st (black) and 30th (red) cycles. Only anodic scans are shown. (b) CVs on Pt(111) in a pure 0.1 M $HClO_4$ solution at 50 mV s^{-1} between 0.05 and 0.95 V. CO had been previously adsorbed at 0.1 V for 15 min on both pristine (red) and cycled (black) samples.

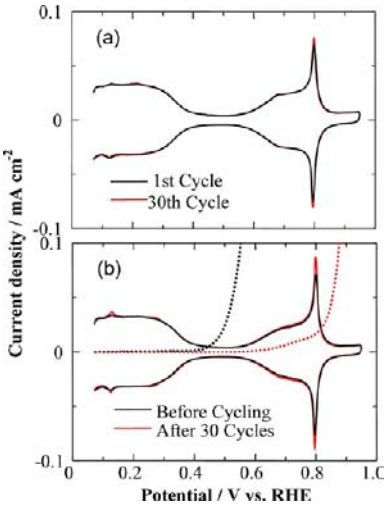

Figure 3. CVs obtained in N_2-saturated 0.1 M $HClO_4$ at 50 mV s^{-1}. (a) Pt(111) cycled between 0.07 and 0.95 V. The 1st (black) and 30th (red) cycles are shown. (b) Pristine Pt(111) (solid black) and Pt(111) previously cycled 30 times in a CO-saturated solution between 0.05 and 0.95 V at 50 mV s^{-1} before CV measurement in pure 0.1 M $HClO_4$ solution (solid red). For reference, the voltammograms for CO-saturated solutions, before potential cycling (black) and after potential cycling (red) from Figure 1c, are shown as dashed lines.

the oxidation main peak, was seen at 0.82 V. After potential cycling, only the main peak was seen at 0.93 V. In Figure 2b, CVs obtained in pure $HClO_4$ are shown, where CO had been previously adsorbed on both the pristine and the cycled samples at 0.1 V for 15 min. Subsequently, the solution was sparged with ultrapure Ar gas for 90 min, and the potential sweeps were carried out from 0.05 to 0.95 V at 50 mV s^{-1} on both surfaces. As clearly seen in Figure 2b, the lower potential CO oxidation current, which had been observed prior to the main peak, disappeared on both the pristine and the cycled surfaces. The peaks for the two samples were both located around 0.85 V. Therefore, without CO in solution, oxidation of CO confined to the surface is believed to proceed similarly on both surfaces.[53,55] The coverage of CO on the pristine electrode was calculated to be 0.66, whereas that on the cycled electrode was 0.69, i.e., a negligible change in surface coverage. During the negative-going scan from 0.95 to 0.05 V, both CVs in Figure 2b showed identical peaks for OH desorption and H adsorption.

Comparing Figure 2a and 2b, the main peaks observed in Figure 2a can be assigned as being associated with oxidation of CO adsorbed on the surface. The origin of the prepeak, therefore, may not be from CO adsorbed on the surface but could be considered to be from oxidation of CO in solution.[82,111] We will discuss this point further in section 3.2.

To try to understand the surface structure of the pristine and cycled Pt(111), CVs were carried out in pure 0.1 M $HClO_4$ in the absence of CO. Figure 3a shows CVs at the 1st and after the 30th potential cycles. A subtle growth of the spikes at around 0.8 V was seen, which is indicative of a small increase in flatness of the terraces.[111] The CVs in Figure 3b were obtained on pristine Pt(111) (solid black) and Pt(111) after the 30 potential cycles in a CO-saturated solution followed by CO stripping (solid red) as in Figure 2b. The spikes at 0.8 V can be seen to have become more established after potential cycling in a CO-saturated solution. Therefore, the electrochemical measurements indicate that although the terraces might become slightly flatter after the potential cycles in CO-saturated solution the changes should be small. The small peaks at 0.12 V are due to hydrogen adsorption/desorption at steps,[118] specifically, (111) steps.[119] The small change seen for these peaks might indicate a change in the step structure. The initial CO oxidation behavior of the uncycled surface as well as that obtained after 30 potential cycles (both from Figure 1c) are shown in Figure 3b for reference. It can be seen clearly that CO oxidation commences on the pristine surface at ca. 0.35 V vs RHE, at which it can be argued that water does not become activated by oxidation to form OH. This is an important point because most published work has assumed that CO oxidation on platinum requires the presence of adsorbed OH.

3.2. STM Measurements on Pt(111) and (10 10 9) with (111) Steps. In order to understand the change in surface structure, we carried out STM measurements in 0.1 M $HClO_4$. Figure 4a is an in situ STM image of the Pt(111) surface used in this study, in $HClO_4$ under N_2 atmosphere, with the surface covered with CO. The scanned area was 200 nm × 200 nm. Even in this wide scanning range, only two monatomic steps were seen, running nearly parallel to each other; thus, a very flat Pt surface was able to be prepared using the infrared image furnace.[45] The (111) steps, which undulate slightly but essentially run in the ⟨110⟩ direction, were inevitably created on the surface by an estimated misscut of 0.1°, according to the step density. Figure 4b shows a structural model for the (111) step. With upper and lower step atoms, a 2-atom wide (111) surface is created along the step, which is thus termed a (111) step, although some authors refer to this type of step as (110).[61,65,67] Figure 4c shows a close-up STM image on the same surface at 0.1 V in a CO-saturated solution, where small spots are clearly seen forming a hexagonal structure with a distance of 0.56 nm; the unit cell is shown by a black rhombus. This surface structure is assigned as the (2 × 2)-3CO structure of CO molecules on Pt(111), where CO is adsorbed with one molecule on top and two at 3-fold sites, as shown in the model

dx.doi.org/10.1021/ja309886p | J. Am. Chem. Soc. 2013, 135, 1476−1490

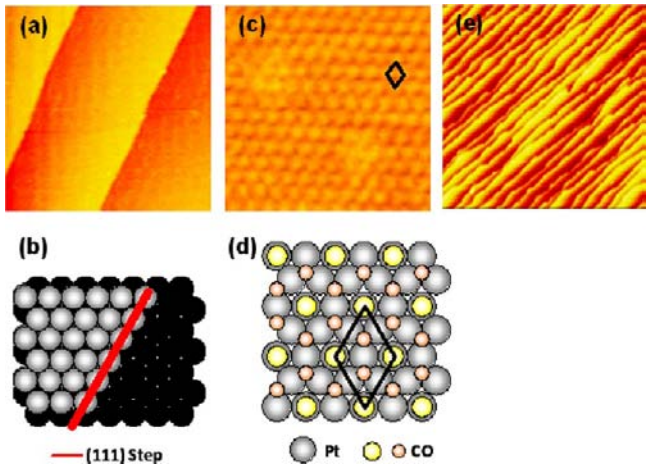

Figure 4. (a) STM image on Pt(111) covered with CO in 0.1 M $HClO_4$ obtained at 0.1 V (200 nm × 200 nm). (b) Structural model of the (111) step. (c) STM image on Pt(111) in CO-saturated 0.1 M $HClO_4$ obtained at 0.60 V (6 nm × 6 nm). Unit cell is shown by the rhombus. (d) Structural model for the (2 × 2) structure of a CO adlayer. (e) STM image on Pt(10 10 9) covered with CO in 0.1 M $HClO_4$ obtained at 0.1 V (100 nm × 100 nm).

in Figure 4d. By STM, only the CO molecules adsorbed at the on-top sites are reported to be observable.[129] In our case also, in Figure 4b, only CO adsorbed at the on-top sites was observed. Figure 4e shows an STM image on Pt(10 10 9), with (111) steps, observed in pure 0.1 M $HClO_4$. Slightly undulating steps are running in the ⟨110⟩ direction. The step separation was observed to be 5 nm, which is very close to the ideal value of 4.67 nm. In this way, the step density was increased by a factor of 20 compared with that on the Pt(111) surface (Figure 4a) used in this study.

To understand the effect of potential cycling in a CO-saturated solution, STM observations were carried out after cycling in the same solution. During potential cycling, the STM tip was withdrawn from the surface to avoid the effect of the local electric field. Figure 5a-1 shows the STM image on Pt(111) before potential cycling in the scanned area of 10 nm × 10 nm. CO is forming the (2 × 2) structure on the terraces. CO is seen to be adsorbed very distinctly on the upper terrace, including the upper edge of the step but much less distinctly on the lower terrace. Locally, the step in the image is not straight but composed of many nanoscale steps and kinks in different directions. Step-adatoms are also found. Figure 5a-2 is a structural model, where the atomic arrangements correspond to those in the oval in the STM image in Figure 5a-1. The red lines indicate the existence of local (111) steps. Figure 5b shows the STM image after 5 potential cycles. The number of kinks and step-adatoms decreased, and the step became somewhat straighter. No difference in the (2 × 2) arrangement of CO molecules was seen on the upper terrace, while the spots became more distinct on the lower terrace. Neither pits nor adatoms were formed on the terrace. Figure 5c-1 shows the STM image of the Pt(111) surface after 30 potential cycles in a CO-saturated $HClO_4$, on which the CO-oxidation prepeak had vanished (Figure 2a). Surprisingly, the (111) step became perfectly straight. To our knowledge, this is the first report that describes the generation of a perfectly straight step. This is made possible by the in situ nature of the experiment.

A related result has been reported by Strmcnik et al., who showed in their ex situ STM work that there was a tendency for straight, parallel steps to be produced, but the steps were not perfectly straight, possibly due to the inevitable loss of potential control in their ex situ measurement. These authors also observed straight steps meeting at 120° angles to be produced during potential cycling in a CO-containing electrolyte of a

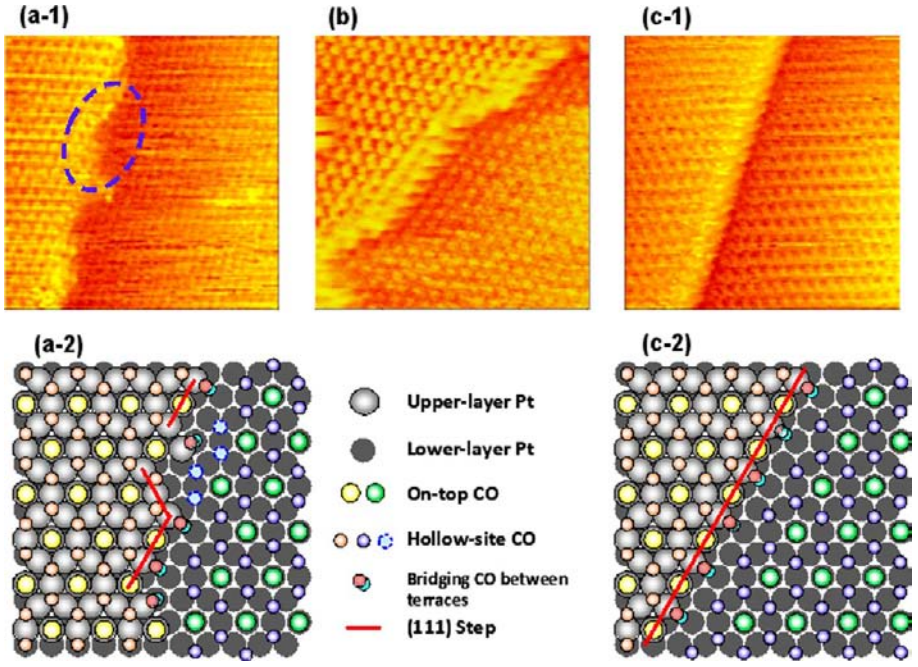

Figure 5. (a-1) STM image on Pt(111) before potential cycling obtained in 0.1 M $HClO_4$ saturated with CO at 0.55 V (10 nm × 10 nm). (a-2) Structural model for a-1. (b) STM image on Pt(111) after 5 potential cycles obtained in 0.1 M $HClO_4$ saturated with CO at 0.55 V (10 nm × 10 nm). (c-1) STM image on Pt(111) after 30 potential cycles obtained in 0.1 M $HClO_4$ saturated with CO at 0.55 V (10 nm × 10 nm). (c-2) Structural model for c-1.

dx.doi.org/10.1021/ja309886p | J. Am. Chem. Soc. 2013, 135, 1476−1490

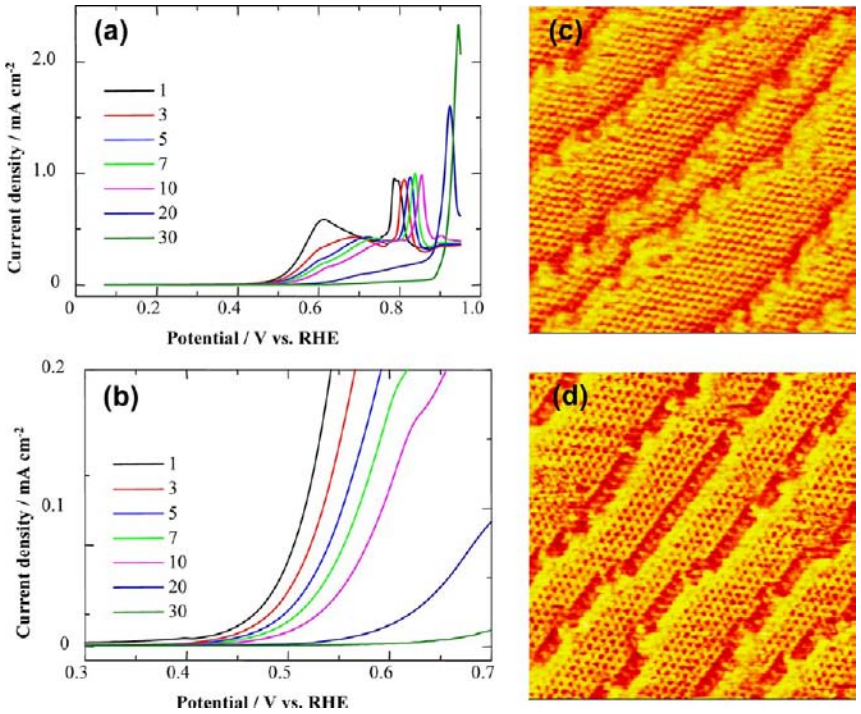

Figure 6. (a) CV on Pt(10 10 9) in a 0.1 M $HClO_4$ solution saturated with CO between 0.07 and 0.95 V at 50 mV s^{-1}. Only anodic scans are shown. (b) Onsets for CO oxidation. (c) STM image on Pt(10 10 9) before potential cycling obtained in 0.1 M $HClO_4$ saturated with CO at 0.55 V (10 nm × 10 nm). (d) STM image on Pt(10 10 9) after 5 potential cycles obtained in 0.1 M $HClO_4$ saturated with CO at 0.55 V (10 nm × 10 nm).

Pt(111) single crystal that initially exhibited an island feature.[81] These authors did not observe the atomic-level nature of the steps that were formed, but on the basis of the present results, it could be assumed that (111) steps were also being formed.

Another related result has been reported very recently by Rudnev and Wandlowski, in which Pt(100) single-crystal surfaces were subjected to various types of gas-phase pretreatments and then subjected to in situ STM and electrochemical CO oxidation measurements.[46] This paper also does not show atomic-resolution results, but the authors propose, on the basis of cyclic voltammetric evidence, the CO-induced restructuring of (110) steps on the (100) surface to form (111) steps, with decreased catalytic activity.

In any case, the present results indicate a strong preference for the (111) step structure to form during cycling to higher potentials in the presence of dissolved CO. We obtained some indications from DFT calculations that help to explain why this happens, as discussed later in this section.

In another somewhat related result, Somorjai and co-workers observed in their gas-phase STM studies with Pt-stepped single crystals that on a Pt(332) surface, with (111) steps that were initially rather straight, the steps remained straight upon exposure to a low-pressure CO atmosphere.[131] These authors rationalized their results, which also include the use of higher CO pressures and more extreme restructuring processes, on the basis of DFT calculations, based principally on changes in overall surface free energy.

In the present work, therefore, the decrease in activity of the CO oxidation at the prepeak can be associated with the transformation of the disordered steps to straight (111) steps. It should be noted that the STM images in Figure 5 were obtained at 0.55 V, i.e., in the range in which steady-state prepeak CO oxidation can be observed. By comparing the CV results presented in Figure 1c, we conclude that CO oxidation must have been proceeding when Figure 5a-1 was obtained. Figure 1a also confirms that maintaining the potential lower than 0.6 V does not lower the activity for the CO oxidation at the prepeak. Interestingly, CO molecules were observed continuously, both on the terraces, particularly the upper terraces approaching steps, when Figure 5a-1 was captured; no movement or replacement of CO on the Pt electrode surface was detected, although the lack of distinct spots on the lower terrace approaching a step could indicate movement of CO. Therefore, we propose that CO oxidation proceeded at locations where CO was not observed by STM, e.g., on the rising part of the step itself or on the lower terrace (right side), close to the step. Since CO was not observed even several atomic rows away from the lower part of the step, it is possible that CO could have been moving quickly and continuously toward the step. We will discuss the possible reaction sites for CO oxidation at lower electrochemical potentials in section 3.5.

We next used the Pt(10 10 9) surface to understand the CO oxidation processes with an increased number of (111) steps. This surface has a nominal terrace width of 20 atoms (4.67 nm). Figure 6a and 6b shows the results for the CVs in a CO-saturated $HClO_4$ solution between 0.07 and 0.95 V, in which only the positive-going scans are shown. Comparing with Figure 1c and 1d, it can be seen that the onset potential moved in the negative direction, namely, from 0.4 V on Pt(111) to 0.3 V on Pt(10 10 9). However, the current density was in a similar range, as seen in Figure 1c, not proportional to the step density and increased by a factor of 20, which might indicate efficient mass transport in both cases. The shapes of the voltammograms in Figures 1c and 6a are similar. After 30 scans, the prepeak for CO oxidation at lower potentials vanished, as was seen on Pt(111). Therefore, the same mechanism may apply to the structural change and the activity decrease on both Pt(111) and (10 10 9).

dx.doi.org/10.1021/ja309886p | J. Am. Chem. Soc. 2013, 135, 1476−1490

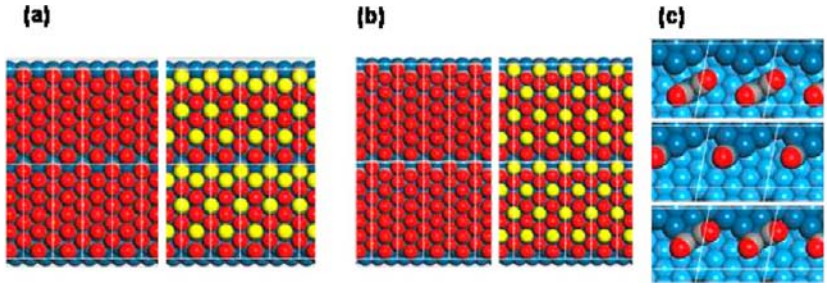

Figure 7. DFT-generated images of high CO coverage [(2 × 2)−3CO adsorbed layer structures on the terraces] for the following: (a) (111) step on a Pt(443) surface (10 CO molecules per unit cell), with on-top CO molecules adsorbed at every other step edge Pt, interspersed with on-top CO molecules on the terrace just below the step itself (top and center of the figure); (b) (100) step on a Pt(10 8 8) surface, with on-top CO molecules adsorbed at every other step edge Pt, interspersed with bridging CO molecules at the step itself (top and center of the figure); (c) proposed structures involved with propagation of (111) steps vs (100) steps, based on the adsorbed $Pt(CO)_2$ (top), which must discard one CO if it continues the (100) step (middle) but can retain it if it continues the (111) step (bottom). (a and b) White lines show the surface unit cells, based on the vertical direction being normal to the surface as a whole rather than the terraces. In the left-hand panels, oxygen atoms of the CO molecules are shown in red, whereas in the right-hand panels, oxygen atoms of the on-top CO molecules have been highlighted in yellow for easier comparison with the STM images.

STM observations were subsequently carried out on Pt(10 10 9). Figure 6c shows the image before cycling and Figure 6d after 5 cycles. The distance between the steps was approximately 5 nm. In Figure 6c, the step lines were undulating, as was seen in Figure 5a-1, with defects on the steps. The (2 × 2) structure of CO is clearly seen on the terraces, and the (111) steps were covered with CO, as previously described in Figure 5. In Figure 6c, the bright spots were observed clearly on the terraces more closely to the lower part of the step, compared with the wide terraces in Figure 5a-1.

After 5 cycles, the steps clearly became composed of nanoscale straight (111) steps, and subsequent cycling led to steps having fewer defects (not shown), as depicted schematically in Figure 5c-1. Notably, neither the number of steps nor the step distribution changed; the steps maintained a distance of 5 nm between each other. Therefore, the decrease in the activity at lower potentials should not be attributed to a decrease in the number of steps but to a change in step morphology; the straight (111) steps became well established. The images were measured at 0.50 V, in the range of the prepeak for CO oxidation, but no movement of CO molecules on the surface was observed. This is consistent with the observation that the prepeak is due to oxidation of solution-phase CO.

DFT calculations were carried out in order to try to understand the fact that the (111) steps were favored in the presence of adsorbed CO. The overall process occurring during potential cycling is quite complicated, and we have not attempted to simulate it in detail but instead have attempted to focus on key aspects that might explain the preference. In section 3.4, we will briefly outline the overall process. The most striking result of the calculations is that, for both types of steps, the CO adsorption arrangement is able to very effectively cover the step, in many cases continuing the pattern on the terrace across to the lower terrace, thereby protecting the step from possible attack by water molecules.

We attempted to take into account the observation that the (111) steps were favored for both wide and narrow terraces, as observed experimentally. Therefore, we considered that the energy should be favored at a very local level for the two types of steps and carried out calculations to determine which sites were the most energetically favored in the step region. For both Pt(322) with (100) steps and Pt(553) with (111) steps, both with 5-row terraces, the Pt atoms in atop sites at the step edge were heavily favored adsorption sites, as reported by others in both theoretical calculations[117] and experimental measurements.[126]

We considered the possibility that the CO adsorption energies in these top sites might be a contributing factor to the preference for (111) steps if the energies differed. In fact, the (100) steps were found to be favored slightly (−55.2 kcal mol^{-1}) compared to the (111) steps (−54.7 kcal mol^{-1}) in our results for Pt(533) and Pt(553), respectively. However, in the gas-phase experimental work of Tränkenschuh et al., on-top CO adsorption was found to be stronger and the coverages higher at the (111) steps on Pt(553) compared to the same sites on the (100) steps on Pt(322), although the differences were not quantified precisely.[126] Also, based on electrochemical and in situ infrared evidence, Chen et al. obtained slightly higher CO coverages on (111) steps compared to (100) steps on several stepped Pt single crystals vicinal to Pt(111).[71] At present, we regard the differences between the two adsorption energies as being rather small, both in our DFT calculations and in the published experimental results, but are continuing to examine them.

We also focused on the energetics of possible individual events in the restructuring process. For example, we examined addition of Pt adatoms at (100) steps, (111) steps, and corners at which a (100) step comes together with a (111) step. This is illustrated in Figure 7c. Essentially we are examining the propagation of (111) vs (100) steps via addition of a single adatom. The clearest example is the corner structure. Depending upon which side of the corner the adatom attaches, either one or the other of the two step structures will be extended. It turns out that in the absence of CO it is slightly more favorable to extend the (100) step, but in the presence of CO, it is significantly more favorable to extend the (111) step. This is because the geometry of the Pt adatom is such that it can simultaneously adsorb two CO molecules in the on-top (linear) configuration, greatly stabilizing it, whereas in the former case, the adatom can only adsorb one single on-top CO. As seen in the Supporting Information, Figure S-1, the geometries of the two types of step-adatom structures are subtly yet distinctly different, even though the nominal coordination numbers (CN) are the same, i.e., five. It should be stressed that, surrounding these adatoms, there would be a

high coverage of CO molecules, which we are not including in some calculations, because their effect will be quite similar in both cases and therefore not instrumental in deciding the adatom attachment site. In the Supporting Information, we also describe the energy calculations in greater detail.

We also considered the possibility that the energetics of various CO adsorption scenarios might be modified significantly in the presence of water and thus examined the effect of adding one or more water molecules per adsorbed CO in some situations. In all cases we examined, the interactions with water led to small increases in the adsorption energy of CO (0.7−0.9 kcal mol^{-1} for atop sites, 1.2−2.7 kcal mol^{-1} for bridge-on-step sites), but the relative trends were preserved. These results were consistent with previous reports involving CO adsorbed on Pt in the presence of water.[140,141]

In Figure 8, we show how the calculated adsorption arrangement of Figure 7a for Pt(443) compares with the

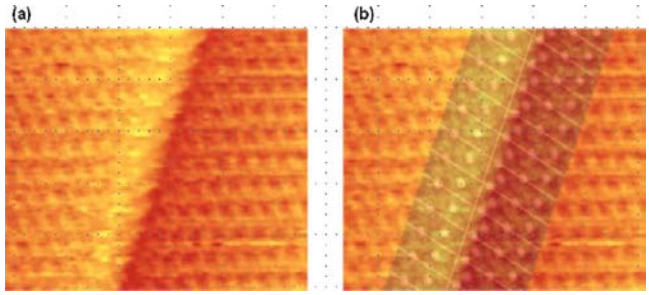

Figure 8. (a) Section of the STM image of the (111) step after potential cycling (ca. 6.3 nm × 6.3 nm); (b) same image overlaid with a light gray pattern of the theoretically calculated Pt(443) surface shown in Figure 7a. Oxygen atoms of the on-top CO molecules have been highlighted, as in the right-hand panel of Figure 7a, to help distinguish them and facilitate comparison with the STM image.

experimentally obtained STM image for the straight (111) step, just in the step region itself, since the number of rows of Pt atoms in the terrace for the calculated structure was only 8, compared to ca. 20 on the actual surface. The correspondence between the experimental STM and the DFT-generated images is excellent. The image on the right (Figure 8b) shows a superposition of the original STM image and a light gray version of the calculated surface. It can be seen that at the positions at which the experimental and computed images coincide the bright spots (atop CO molecules) appear brighter. The correspondence, although not perfect, lends strong support to the computed model.

Although we have chosen these particular CO adsorption patterns in order to match the STM images, we note that there are other possible patterns with similar overall energies. However, after matching the patterns on the terraces, the possible step structures become limited to basically two choices, one involving a bridging CO on the step itself and the other not. This choice is difficult to decide based on the STM images. In any case, the computed energies are believed to be rather reliable, based on the all-electron, relativistic calculations used here, even though the absolute values are known to be somewhat overestimated.[142] This overestimation might tend to slightly enhance the stability of the high-coverage (2 × 2)-3CO structure, a point we will take up separately in the near future. We also briefly mention the influence of the presence of water below. However, we note that there should not be any other overt perturbing influences, such as possible potential-induced effects, that could upset the comparison of the DFT calculations and the STM-based structures, because the effective surface potential for the calculations, carried out with a neutral (uncharged) Pt slab, can be considered to be very close to that at which water molecules are found to change their orientation from H down to H up (ca. 0.35 V vs RHE),[143] because our calculations show water molecules adsorbing on the Pt(111) terrace in a nearly horizontal configuration (see Figure S-1, Supporting Information).[149] More detailed results on this point will also be reported separately in the near future.

The gas-phase measurements of Tränkenschuch et al. in which CO adsorption was compared for Pt(322) and Pt(553) provide very useful information on the energies, coverage, arrangements, and temperature dependences of on-top and bridging CO.[126] We note that, in that study, the coverages were significantly smaller than in the present, aqueous-phase results. As already mentioned, the presence of water strengthens the adsorption of CO on Pt, and increasing numbers of water molecules continue to strengthen the adsorption, so that such effects certainly must be considered in future work. In fact, such effects can be extremely important and help to stabilize the high-coverage (2 × 2)-3CO adlayer structures that we observed in all of our images. This effect was emphasized, for example, in the experimental work of Ito and co-workers.[102] Also, in the future, calculations must be carried out to try to simulate the actual events occurring in the step region during potential cycling, with the effects of water molecules and electrochemical potential included.[144−146]

3.3. Electrochemical and STM Measurements on Pt(20 19 19) with (100) Steps. After examining the (111) steps, we investigated Pt(20 19 19), i.e., a (111)-oriented surface with terraces that are 39 atoms wide, with (100) steps. Figure 9a

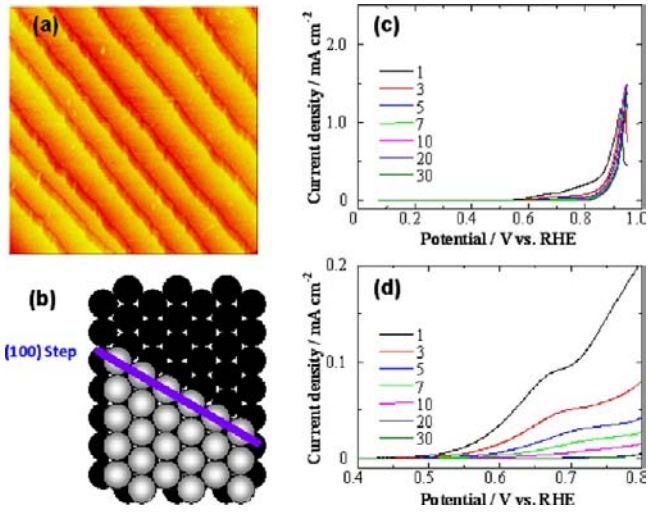

Figure 9. (a) STM image on Pt(20 19 19) covered with CO in 0.1 M $HClO_4$ obtained at 0.1 V (100 nm × 100 nm). (b) Structural model of the (100) step. (c) CVs on Pt(20 19 19) in a 0.1 M $HClO_4$ solution saturated with CO between 0.07 and 0.95 V at 50 mV s^{-1}. Only anodic scans are shown. (d) Onsets for CO oxidation.

shows the STM image of Pt(20 19 19) covered with CO in pure 0.1 M $HClO_4$ obtained at 0.1 V. Theoretically, the distance between two steps is 8.9 nm, and the average distance obtained in the STM image was approximately 9 nm. Figure 9b is a structural model for the (100) step, where a 2-atom wide (100) surface is created along the step.

dx.doi.org/10.1021/ja309886p | J. Am. Chem. Soc. 2013, 135, 1476−1490

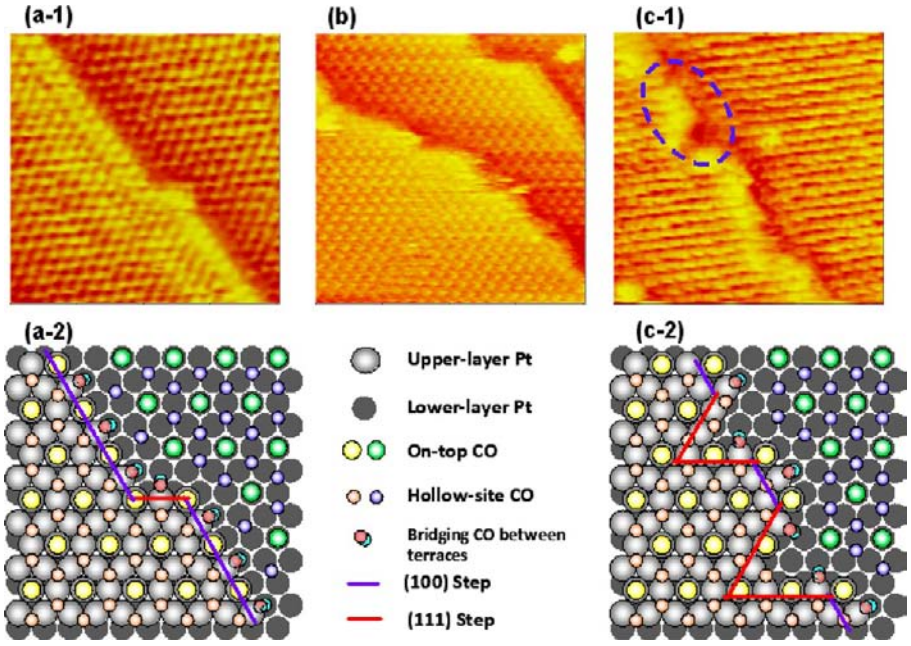

Figure 10. (a-1) STM image on Pt(20 19 19) before potential cycling obtained in 0.1 M $HClO_4$ saturated with CO at 0.55 V (10 nm × 10 nm). (a-2) Structural model for a-1. (b) STM image on Pt(20 19 19) after 5 potential cycles obtained in 0.1 M $HClO_4$ saturated with CO at 0.55 V (10 nm × 10 nm). (c-1) STM image on Pt(20 19 19) after 30 potential cycles obtained in 0.1 M $HClO_4$ saturated with CO at 0.55 V (10 nm × 10 nm).

We carried out continuous CV measurements in a CO-saturated $HClO_4$ solution for 30 cycles, in the same way as we did on Pt(111) and (10 10 9) with (111) steps. The results are summarized in Figure 9c, showing only the anodic scans. Compared with Figures 1c and 6a, the onset potential for CO oxidation was much higher, namely, 0.5 V. The current density was also smaller. Therefore, the activity for CO electrooxidation in the prepeak region was lower than that on Pt(111) surfaces with (111) steps. As the number of cycles increased, the prepeak became smaller and vanished after 30 cycles, as was the case with the (111) steps, but the rate of the decrease in activity was faster on Pt(20 19 19), with (100) steps.

In order to examine the changes in surface structures, STM observations were again carried out. Figure 10a-1 shows an STM image on Pt(20 19 19) in $HClO_4$ saturated with CO. Surprisingly, the step line was rather straight, mostly with (100) steps, with a small number of (111) steps. Figure 10a-2 shows a structural model that was constructed from the image in Figure 10a-1. A very small number of defect sites were found. This could explain the initial low activity for the CO electrooxidation in the prepeak region. In the middle of the model in Figure 10a-2, a local (111) step is sandwiched between (100) steps, i.e., a kink, as seen in the STM image in Figure 10a-1. We refer to the Pt atom at the outside corner of the kink as a kink site.

DFT calculations indicated that a highly stable arrangement of CO molecules can be achieved for the (100) steps with terraces containing 5, 9, 13, etc., rows, so that the pattern repeats from one terrace to the next. For the Pt(10 8 8) surface, with 9 row terraces, the CO molecules adsorbed in the step region are shown in the center of Figure 7b. We hypothesized that this type of pattern can be propagated in both directions away from the step; this appears to actually be the case when we compare the STM image with the calculated Pt(10 8 8) structure in the (100) step region (Figure 11). Again, the degree of correspondence is excellent.

Figure 10b shows the STM image after 5 cycles. In contrast to the result on the surface with (111) steps (Figures 5 and 6),

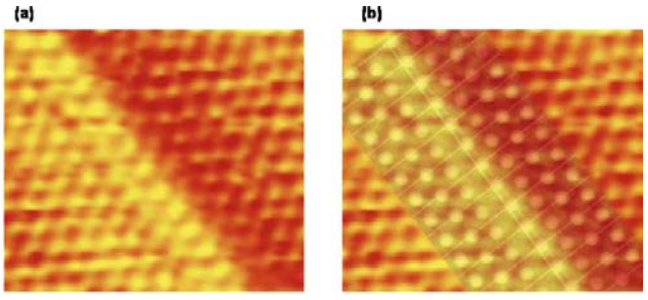

Figure 11. (a) Section of the STM image of the (100) step before potential cycling (ca. 5.2 nm × 5.2 nm); (b) same image overlaid with a light gray pattern of the theoretically calculated Pt(10 8 8) structure shown in Figure 7b. The oxygen atoms of the on-top CO molecules have been highlighted, as in the right-hand panel of Figure 7b, to help distinguish them and to facilitate comparison with the STM image.

the straightness of the step was lost and the step clearly began to undulate. This is very different from the results with (111) steps. Figure 10c-1 shows the step morphology after 30 potential cycles. The step looks zigzagged and at first sight disordered. However, a closer look at the image reveals that the step has excellent regularity. Figure 10c-2 shows a structural model derived from Figure 10c-1, which is also based indirectly on the DFT results. After potential cycling, local (111) steps were introduced into the (100) steps and the step is now composed of local (100) and (111) steps, where the (111) steps are rather predominant. In the case of Pt(111) and Pt(10 10 9), the (111) steps became straight, increasing the density of (111) steps (Figure 12a). On the other hand, on the Pt(20 19 19) surface, the steps became less straight but the proportion of local (111) steps increased (Figure 12b). In both cases, i.e., for (111) and (100) steps, the proportion of local (111) steps increased and the CO oxidation rate in the prepeak region decreased.

dx.doi.org/10.1021/ja309886p | J. Am. Chem. Soc. 2013, 135, 1476−1490

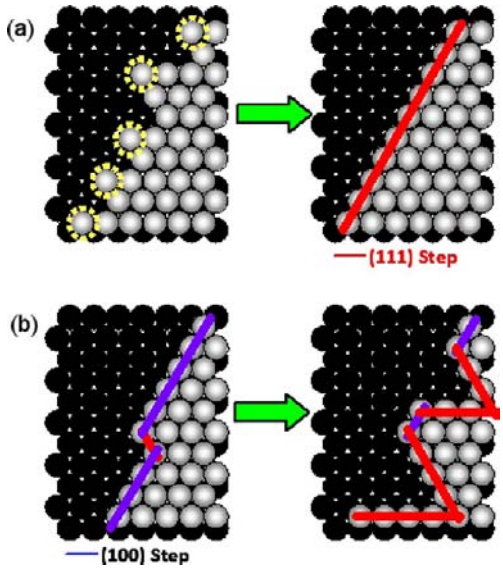

Figure 12. Structural models for transformation of (111) (a) and (100) (b) steps after potential cycling in a CO-saturated solution.

The number of low-coordination kink sites increased, but the CO oxidation activity decreased, which was very surprising. We found that the CO adsorption patterns at high coverage are able to continue across such a step without significant perturbation, so that the kink sites are protected. We hypothesize that the initial CO oxidation activity of the (100) step might be due to a small number of isolated step-adatoms, which perturb the ordered adsorbate structure.

In related gas-phase experiments, Somorjai and co-workers observed that a Pt(557) single-crystal surface, initially with straight (100) steps, began to exhibit wavy steps after exposure to low-pressure CO.[131] In fact, upon exposure to higher pressure CO, the whole surface broke up into highly oriented triangular nanocrystals, such that the (111) step geometry was maximized.

3.4. Proposed Overall Mechanism for Step Restructuring. Even though we focused on what we propose might be the key event in the restructuring process, it is necessary to place this into an overall scenario for the events occurring in the electrochemical potential cycling. During the positive-going potential sweep, it is probable that the platinum surface becomes oxidized in stages preferentially at the steps, first to a hydroxylated form and then an oxygenated form at higher potentials. Recently, these processes have received renewed attention both experimentally[131] and theoretically[128,133] and are becoming better understood.

Referring to Figure 1, we can see that the CO oxidation behavior does not change until the potential is swept to 0.8 V vs RHE, i.e., the potential at which the sudden oxidation of CO adsorbed on terraces occurs, presumably associated with the process responsible for the sharp peak at a similar potential that occurs in the absence of CO, which has been assigned to the initial oxidation of the Pt(111) terraces with adsorption of OH.[119] Thus, it appears to be a prerequisite to remove adsorbed CO before oxidation of the steps can proceed. Electrochemical oxidation of Pt is known to occur preferentially at steps.[131−133] These studies have noted that the (100) and (111) steps on Pt(111) are oxidized at slightly different potentials and rates. Björling et al. point out that conversion of OH to O occurs in the 0.8−1.0 V range in 0.1 M $HClO_4$, prior to the large anodic peak at 1.0 V for this process on the (111) terraces.[131] Although there are some differences in the behavior at the two types of steps, if the sweep is reversed at 0.95 V, we can probably assume that the process involves either of the following reactions on both steps

$$Pt(OH)_2 \rightarrow PtO_2 + 2H^+ + 2e^- \quad (1)$$

$$PtO + H_2O \rightarrow PtO_2 + 2H^+ + 2e^- \quad (2)$$

with the standard potential for the latter being given as 1.045 − 0.0591pH.[134]

When the potential is reversed at 0.8 V, either $Pt(OH)_2$ or PtO can be dissolved to produce the square planar complex $Pt(H_2O)_4^{2+}$.[135] Alternatively, if the potential is swept to 0.95 V, the resulting PtO_2 can be reduced to form the same complex

$$PtO_2 + 2H_2O + 4H^+ + 2e^- \rightarrow Pt(H_2O)_4^{2+} \quad (3)$$

with a standard potential of 0.837 − 0.118pH − 0.030 $\log[Pt(H_2O)_4^{2+}]$.[134,135]

By analogy with the substitution reactions of the tetraaquo dication with chloride, which are well known,[136] the former could react with CO, in principle, to produce the square planar cationic complex $Pt(CO)_4^{2+}$, which is known.[137] Alternatively, a Pt adatom can be reductively deposited on the terrace as $Pt(CO)_2$, as shown in Figure 7c (top). The corresponding $Rh(CO)_2$ species has been identified spectroscopically,[138] but it has never been reported for Pt. We carried out DFT calculations on this species and found it to be stable. The two CO molecules bind quite strongly to this adatom (−48.9 kcal mol^{-1}), so that its bonding to the surface becomes weakened, which would make it more mobile than usual. In either case (ion or neutral atom), the single atomic Pt species would then have the opportunity to redeposit at the nearby step in an energetically favorable configuration. According to our DFT calculations, we expect that the resulting step-adatom would retain both COs if it were attached to a (100) step but would have to eject one CO if it were attached to a (111) step (Table S-1, Supporting Information) due to the respective bonding characteristics (Figure S-1, Supporting Information). The same characteristics would be observed if the adatom were to attach at a corner between a (100) step and a (111) step, as shown previously in Figure 7c (bottom) and Figure 7c (middle).

3.5. Active Sites for CO Oxidation in the Prepeak Potential Region. After potential cycling, the CO oxidation activity at potentials lower than 0.7 V was completely lost, associated with the morphological change of the steps. In this section, we will discuss the possible active sites for the CO electrooxidation reaction.

From our experiments, the CO oxidation activities of the various types of steps in the prepeak potential region decreased in the following order: (111) step with defects > straight (100) step > (100) step with (111) local steps ≈ (111) straight step.

As a first guess, one might assume that the active sites for CO oxidation in the low-potential region are undercoordinated defect sites, and in fact, this is quite likely. This is also similar to the conclusion reached by Strmcnik et al.[81] and also by Rudnev and Wandlowski.[46] We believe that this is a reasonable idea, due to the greatly enhanced bonding possibilities for both CO and water. However, this assumption is not sufficient to explain all of the present results. Specifically, there are two facts that could lead one to question this assumption: (1) in the case of Pt(20 19 19), the number of defects or undercoordinated sites

actually increased (Figure 10) while the activity decreased (Figure 9); (2) during CO oxidation, the steps were completely covered with CO, and they were very stably observed by STM images. As already mentioned, based on our DFT calculations, the adsorption energy of CO is very high at the step edge (on-top) sites (ca. −55 kcal mol^{-1}). Therefore, it appears that the on-top sites at the upper edge of the steps may not be open for the CO oxidation reaction, at least for straight steps. However, as discussed later in more detail, there could be two exceptions: (1) a single isolated adatom adsorbed at an otherwise straight step or (2) a kink site.

CO is oxidized electrochemically in the presence of H_2O as in eq 4[113]

$$CO + H_2O \rightarrow CO_2 + 2H^+ + 2e^- \quad (4)$$

Therefore, not only the adsorption site for CO but also that for H_2O must be considered; the latter can become oxidized to OH at higher potentials,[54,61,67] but as we have shown here, *that event may not be absolutely required to initiate CO oxidation*.

Figure 2a is very indicative. On the surface that exists after potential cycling, CO oxidation is associated with CO adsorbed on the entire surface. This means that H_2O molecules penetrate the rigid CO layer to the platinum surface for reaction 4 to proceed. On the other hand, before potential cycling, the fact that CO starts to be oxidized prior to the main surface CO oxidation could mean that, on the lower terrace close to the step, for example, there might be some vacant sites or at least sites with weakly adsorbed CO, which might be available for H_2O adsorption, even on a surface that is mostly covered with CO.

Since the terraces and upper edges of the steps were found to be completely covered with CO in CO-saturated solution, it was considered to be more fruitful to entertain the possibility that an open site could exist just below the edge of a step. On as-prepared, pristine surfaces (before the potential cycling), this type of site could be open, without a CO molecule, or, at least, the CO molecules might be bound more weakly. In Figure 5a-2 and 5c-2, schematic models for the CO adsorption are shown, based on the STM data in Figure 5a-1 and 5c-1, respectively, taking into account the van der Waals diameters. Clearly, in Figure 5c-1, several examples of possible vacant 3-fold sites are seen on the lower terrace close to the step (shown as dashed circles). These can exist due to the disruption of the long-range order that is evident on the main part of the terrace. Thus, it becomes sterically difficult for CO molecules to adsorb at such sites due to the proximity to the disordered step. We propose that, even if CO can adsorb, water can also compete for adsorption at adjacent atop sites, being slightly less bulky. Once adsorbed, it can be in a favorable position to participate in the oxidation of a CO molecule, which could be adsorbed at an isolated step-adatom, or at a kink site, or on the lower terrace, as seen in Figure 5a-2. Thus, a water molecule could momentarily adsorb close to the step, react with a neighboring CO, and both would then desorb in the form of CO_2, making these sites available for continuation of the reaction between CO and H_2O in solution. In this reaction model, only the geometric effect is being considered, with chemical effects being neglected. Clearly, the latter must also be considered in future work.

For completeness, we would also like to propose two other alternatives. First, water molecules could also adsorb at low coordination Pt atoms such as step-adatoms. We obtained very high adsorption energies at on-top configurations on step-adatoms (−18.3 kcal mol^{-1} at the (100) step-adatom and −24.0 kcal mol^{-1} at the (111) step-adatom) compared to corresponding on-top configurations on the steps themselves (−16.5 kcal mol^{-1} on (100) steps and −16.4 kcal mol^{-1} on (111) steps) and on flat terraces (−8.8 kcal mol^{-1} on the Pt(111) surface). Second, as shown by Santana and Ishikawa, water molecules can hydrogen bond selectively to bridging CO,[140,141] and thus at the rising sections of steps, where such bridging CO molecules would be oriented at angles significantly away from normal to the surface, this could possibly assist CO oxidation. This would allow water to react directly from solution in a so-called Eley−Rideal mechanism.[60,128]

Summarizing these purely geometric effects, for the perfect (111) step edges, CO molecules can adsorb with a highly regular surface arrangement, going continuously from the upper terrace, across the step, to the lower terrace, without a gap, consistent with the STM image in Figure 5c-1 and the calculated configuration in Figure 7a. Specifically, the vacant on-top step sites (lying between those with adsorbed CO) are well protected by adjacent CO molecules as well as the on-top sites below the step. We propose that this is the reason for the very low reactivity of the CO-covered (111) step as well as the restructured (100) step. Clearly, when step-adatom sites exist, there are lapses in this protective shield, so that water could (1) adsorb momentarily at sites on the lower terrace very close to the step, as suggested in Figure 5a-2, (2) possibly adsorb at step-adatom sites close to sites where CO is also adsorbed, or (3) hydrogen bond to a bridging CO at a step-adatom.

For the initially nearly perfect (100) step, we propose that the intermediate reactivity might be due to the possible presence of small numbers of isolated step-adatoms, which would perturb the robust protective shield and could act as active sites, either for CO or water adsorption. However, the reactivity is considered not to be high due to the small number of such adatoms and the rather effective protection of the CO adsorbate layer in the straight step sections. In the case of the (100) step that has been cycled to produce (111) indentations, it appears that even though there are apparent defects the adsorbate layer is able to accommodate itself without allowing completely vacant sites to exist, as shown in Figure 10c-2, and due to the increased presence of (111) steps, there is a higher overall level of protection. Interestingly, in the micro-indentations with (111) steps, it appears, based indirectly on DFT results, that the local environment could be highly hydrophobic. Calculations are being carried out in continuing work to test this hypothesis.

At this point, we are unable to state with certainty what the precise catalytic reaction mechanisms or active sites are. However, we are able to state unequivocally that the highest activity is associated with low-coordination Pt adatoms at the disordered (111) step, because we observed these directly with in situ STM and measured the electrochemical activity that is exhibited in their presence. It is also possible that similar step-adatoms at (100) steps might also lead to high activity, but these were observed more rarely. The activity associated with kink sites on (100) steps was not possible to observe directly, because they were so well protected by the ordered CO adsorbate layer.

Interestingly, the (111) step has been designated as the most active site in gas-phase CO + O oxidation studies, in which the oxygen source is O_2,[147,148] although a recent theoretical study has proposed that decreasing CN is associated with decreasing catalytic activity for Pt.[116] In the electrochemical environment,

(111) terraces, with CN = 9, are considered to be the least active.[81] Several electrochemical studies have also identified steps as having the highest activity.[52,54,62,64,71] However, in essential agreement with other recent studies,[46,81] we found, for the high CO coverage conditions prevailing when CO is present in solution, that the (111) terraces (CN = 9), steps (CN = 7), and kinks (CN = 6) are all associated with very low apparent activity, whereas disordered Pt atoms at the (111) step, including step-adatom sites (CN = 5), are associated with extremely high activity at low potentials.

A summary of the main points that can be made regarding the possible candidates for active sites follows.

1. Even though it has been stated in the gas-phase catalysis literature that (111) steps are most active for CO oxidation,[147,148] we can now show with certainty that, in the electrochemical environment, perfect (111) steps are associated with the lowest activity, due to the high degree of uniformity of the CO adlayer across the step at high CO coverage in the presence of water.
2. The highest activity for CO oxidation can confidently be associated with (111) steps with step-adatoms, due to the disruption of the protective CO adlayer and possibly the sites themselves having intrinsic catalytic activity. It is quite likely that the corresponding sites at (100) steps would also lead to high activity, which may help to explain the initial CO oxidation activity of the nearly straight (100) steps.
3. The catalytic activities appear to generally increase with decreasing coordination number, as proposed by Strmcnik et al.[81] and by Rudnev and Wandlowski[46] for electrochemical CO oxidation, not decrease, as proposed for gas-phase CO + O reactions, with decreasing coordination number.[116]
4. At present, it is not clear whether kink sites at restructured (100) steps are associated with high activity or not. They might promote activity under certain conditions but apparently not at high CO coverages due to the protective CO layer. This question is being addressed in continuing work.

As a final note, we emphasize that we have not explicitly considered the case of adsorbed CO oxidation (stripping), as it would have been beyond the scope of the present work. This process also involves complications, such as the absolute necessity of considering water activation to form OH, as well as the surface diffusion of CO, as discussed extensively in the literature.[61,64,71,105,128]

4. CONCLUSIONS

The relationship between the activity for the electrooxidation of CO in a CO-saturated solution and the morphology of steps at single-crystal Pt(111) electrode surfaces was investigated by electrochemical measurements and STM. On all surfaces investigated, the electrocatalytic activity in the prepeak region decreased after potential cycling between 0.07 and 0.95 V. By STM measurements, it was revealed that the proportion of the step edges that were composed of straight (111) steps increased at all surfaces, irrespective of the initial step composition. DFT calculations have enabled us to suggest reasons why the (111) step is preferred, in the presence of CO, in comparison to the (100) step. After the step edges are either straightened, as in the case of initial (111) steps, or converted to zigzag steps with local (111) steps, as in the case of initial (100) steps, there was a drastic lowering of the electrocatalytic activity. It is proposed that the differences in the morphology at these steps control the absorbability of water molecules on Pt(111) surfaces covered with CO. This idea is supported by DFT calculations, which indicated the configurations of highly stable CO adsorbate structures in the vicinity of both types of steps, which are consistent with the STM images. We believe that, for the first time, we directly clarified using in situ STM, supported by theoretical calculations together with electrochemical measurements, the relationships between the atomic-level structures at the steps on the Pt(111) surface and the activity toward CO electrooxidation. The key result is that the reason for the extremely high catalytic activity of the pristine, disordered (111) step is the presence of poorly coordinated Pt step-adatoms, which both severely disrupt the supremely protective CO adlayer and also possibly act as catalytic sites. We believe that the present work points the way to setting a new standard for direct comparison of surface structure and electrocatalytic activity.

■ ASSOCIATED CONTENT

Supporting Information

Description of the DFT methods used, table of adsorption energies, and detailed images of the structures used in the calculations. This material is available free of charge via the Internet at http://pubs.acs.org.

■ AUTHOR INFORMATION

Corresponding Author

E-mail: jinukai@yamanashi.ac.jp (J.I.); h-uchida@yamanashi.ac.jp (H.U.); m-watanabe@yamanashi.ac.jp (M.W.)

Notes

The authors declare no competing financial interest.

■ ACKNOWLEDGMENTS

This study was supported by a Grant-in-Aid for Scientific Research (KAKENHI) and the New Energy and Industrial Technology Development Organization (NEDO), Japan. The authors are grateful to Prof. Nagakazu Furuya of the University of Yamanashi for the stepped-sample preparation, to Mr. Shuichi Asizawa of the University of Yamanashi for his help in the STM measurements, and to Dr. Kiyoshi Yagi of Riken for the design and setup of the computational cluster.

■ REFERENCES

(1) Guo, X. C.; Madix, R. J. *J. Phys. Chem. B* **2003**, *107* (14), 3105−3116.
(2) Guo, X. C.; Madix, R. J. *Acc. Chem. Res.* **2003**, *36* (7), 471−480.
(3) Besenbacher, F.; Lauritsen, J. V.; Wendt, S. *Nano Today* **2007**, *2* (4), 30−39.
(4) Bowker, M. *Phys. Chem. Chem. Phys.* **2007**, *9* (27), 3514−3521.
(5) Somorjai, G. A.; York, R. L.; Butcher, D.; Park, J. Y. *Phys. Chem. Chem. Phys.* **2007**, *9* (27), 3500−3513.
(6) Somorjai, G. A.; Frei, H.; Park, J. Y. *J. Am. Chem. Soc.* **2009**, *131* (46), 16589−16605.
(7) Somorjai, G. A.; Aliaga, C. *Langmuir* **2010**, *26* (21), 16190−16203.
(8) Hahn, J. R.; Ho, W. *Phys. Rev. Lett.* **2001**, *87* (16).
(9) Katano, S.; Kim, Y.; Hori, M.; Trenary, M.; Kawai, M. *Science* **2007**, *316* (5833), 1883−1886.
(10) Kaji, K.; Yau, S. L.; Itaya, K. *J. Appl. Phys.* **1995**, *78* (9), 5727−5733.
(11) Shinotsuka, N.; Sashikata, K.; Itaya, K. *Surf. Sci.* **1995**, *335* (1−3), 75−82.

(12) Yamada, T.; Batina, N.; Itaya, K. *J. Phys. Chem.* **1995**, *99* (21), 8817−8823.
(13) Wan, L.-J.; Yau, S.-L.; Itaya, K. *J. Phys. Chem.* **1995**, *99* (23), 9507−9513.
(14) Itaya, K. *Prog. Surf. Sci.* **1998**, *58* (3), 121−247.
(15) Zou, S.; Villegas, I.; Stuhlmann, C.; Weaver, M. J. *Electrochim. Acta* **1998**, *43* (19−20), 2811−2824.
(16) Wan, L.-J.; Hara, M.; Inukai, J.; Itaya, K. *J. Phys. Chem. B* **1999**, *103* (33), 6978−6983.
(17) Wan, L.-J.; Suzuki, T.; Sashikata, K.; Okada, J.; Inukai, J.; Itaya, K. *J. Electroanal. Chem.* **2000**, *484* (2), 189−193.
(18) Okada, J.; Inukai, J.; Itaya, K. *Phys. Chem. Chem. Phys.* **2001**, *3* (16), 3297−3302.
(19) Yoshimoto, S.; Tsutsumi, E.; Honda, Y.; Murata, Y.; Murata, M.; Komatsu, K.; Ito, O.; Itaya, K., *Angew. Chem., Int. Ed.* **2004**, *43* (23), 3044-3047.
(20) Sato, K.; Yoshimoto, S.; Inukai, J.; Itaya, K. *Electrochem. Commun.* **2006**, *8* (5), 725−730.
(21) Funtikov, A. M.; Linke, U.; Stimming, U.; Vogel, R. *Surf. Sci.* **1995**, *324* (2), L343−L348.
(22) Funtikov, A. M.; Stimming, U.; Vogel, R. *J. Electroanal. Chem.* **1997**, *428* (1−2), 147−153.
(23) Fujishima, A.; Zhang, X.; Tryk, D. A. *Surf. Sci. Rep.* **2008**, *63* (12), 515−582.
(24) Wendt, S.; Sprunger, P. T.; Lira, E.; Madsen, G. K. H.; Li, Z.; Hansen, J. Ø.; Matthiesen, J.; Blekinge-Rasmussen, A.; Lægsgaard, E.; Hammer, B.; Besenbacher, F. *Science* **2008**, *320* (5884), 1755−1759.
(25) Dohnálek, Z.; Lyubinetsky, I.; Rousseau, R. *Prog. Surf. Sci.* **2010**, *85* (5−8), 161−205.
(26) Henderson, M. A. *Surf. Sci. Rep.* **2011**, *66* (6−7), 185−297.
(27) Lira, E.; Hansen, J. Ø.; Huo, P.; Bechstein, R.; Galliker, P.; Lægsgaard, E.; Hammer, B.; Wendt, S.; Besenbacher, F. *Surf. Sci.* **2010**, *604* (21−22), 1945−1960.
(28) Wang, Z.-T.; Aaron Deskins, N.; Lyubinetsky, I. *J. Phys. Chem. Lett.* **2011**, *3* (1), 102−106.
(29) Bikondoa, O.; Pang, C. L.; Ithnin, R.; Muryn, C. A.; Onishi, H.; Thornton, G. *Nat. Mater.* **2006**, *5* (3), 189−192.
(30) Zhang, Z.; Bondarchuk, O.; White, J. M.; Kay, B. D.; Dohnálek, Z. *J. Am. Chem. Soc.* **2006**, *128* (13), 4198−4199.
(31) Zhang, Z.; Bondarchuk, O.; Kay, B. D.; White, J. M.; Dohnálek, Z. *J. Phys. Chem. C* **2007**, *111* (7), 3021−3027.
(32) Besenbacher, F.; et al. http://owww.phys.au.dk/spm/.
(33) Strbac, S.; Maroun, F.; Magnussen, O. M.; Behm, R. J. *J. Electroanal. Chem.* **2001**, *500* (1−2), 479−490.
(34) Magnussen, O. M.; Zitzler, L.; Gleich, B.; Vogt, M. R.; Behm, R. J. *Electrochim. Acta* **2001**, *46* (24−25), 3725−3733.
(35) Polewska, W.; Behm, R. J.; Magnussen, O. M. *Electrochim. Acta* **2003**, *48* (20−22), 2915−2921.
(36) Magnussen, O. M.; Hageböck, J.; Hotlos, J.; Behm, R. J. *Faraday Discuss.* **1992**, *94*, 329−338.
(37) Magnussen, O. M. *Chem. Rev.* **2002**, *102* (3), 679−726.
(38) Matsushima, H.; Taranovsky, A.; Haak, C.; Grunder, Y.; Magnussen, O. M. *J. Am. Chem. Soc.* **2009**, *131* (30), 10362−10363.
(39) Ye, J. H.; Kaji, K.; Itaya, K. *J. Electrochem. Soc.* **1996**, *143* (12), 4012−4019.
(40) Ando, S.; Suzuki, T.; Itaya, K. *J. Electroanal. Chem.* **1996**, *412* (1−2), 139−146.
(41) Teshima, T.; Ogaki, K.; Itaya, K. *J. Phys. Chem. B* **1997**, *101* (11), 2046−2053.
(42) Ando, S.; Suzuki, T.; Itya, K. *J. Electroanal. Chem.* **1997**, *431* (2), 277−284.
(43) Magnussen, O.; , et al. http://www.atomic-movies.uni-kiel.de/.
(44) Wakisaka, M.; Ohkanda, T.; Yoneyama, T.; Uchida, H.; Watanabe, M. *Chem. Commun.* **2005**, *21*, 2710−2712.
(45) Wakisaka, M.; Asizawa, S.; Yoneyama, T.; Uchida, H.; Watanabe, M. *Langmuir* **2010**, *26* (12), 9191−9194.
(46) Rudnev, A. V.; Wandlowski, T. *Russ. J. Electrochem.* **2012**, *48*, 259−270.
(47) Markovic, N. M.; Ross, P. N. *Surf. Sci. Rep.* **2002**, *45* (4−6), 117−229.
(48) Koper, M. T. M.; Lai, S. C. S.; Herrero, E., Mechanisms of the Oxidation of Carbon Monoxide and Small Organic Molecules at Metal Electrodes. In *Fuel Cell Catalysis*; John Wiley & Sons, Inc.: New York, 2008; pp 159−207.
(49) Korzeniewski, C.; Climent, V.; Feliu, J. M. Electrochemistry at Platinum Single Crystal Electrodes. In *Electrochemistry: A Series of Advances*; Bard, A. J., Zoski, C., Eds.; CRC Press: Boca Raton, FL, 2012; Vol. *24*, pp 75−169.
(50) Lopez-Cudero, A.; Cuesta, A.; Gutierrez, C. *J. Electroanal. Chem.* **2006**, *586* (2), 204−216.
(51) Cuesta, A. *Surf. Sci.* **2004**, *572* (1), 11−22.
(52) Cuesta, A.; Couto, A.; Rincon, A.; Perez, M. C.; Lopez-Cudero, A.; Gutierrez, C. *J. Electroanal. Chem.* **2006**, *586* (2), 184−195.
(53) Cuesta, A.; Perez, M. d. C.; Rincon, A.; Gutierrez, C. *ChemPhysChem* **2006**, *7* (11), 2346−2351.
(54) Lopez-Cudero, A.; Cuesta, A.; Gutierrez, C. *J. Electroanal. Chem.* **2005**, *579* (1), 1−12.
(55) Rhee, C. K.; Feliu, J. M.; Herrero, E.; Mrozek, P.; Wieckowski, A. *J. Phys. Chem.* **1993**, *97* (38), 9730−9735.
(56) Orts, J. M.; Fernandez-Vega, A.; Feliu, J. M.; Aldaz, A.; Clavilier, J. *J. Electroanal. Chem.* **1992**, *327* (1−2), 261−278.
(57) Angelucci, C. A.; Herrero, E.; Feliu, J. M. *J. Solid State Electrochem.* **2007**, *11* (11), 1531−1539.
(58) Vidal-Iglesias, F. J.; Solla-Gullon, J.; Campina, J. M.; Herrero, E.; Aldaz, A.; Feliu, J. M. *Electrochim. Acta* **2009**, *54* (19), 4459−4466.
(59) Rodes, A.; Gomez, R.; Feliu, J. M.; Weaver, M. J. *Langmuir* **2000**, *16* (2), 811−816.
(60) Bergelin, M.; Herrero, E.; Feliu, J. M.; Wasberg, M. *J. Electroanal. Chem.* **1999**, *467* (1−2), 74−84.
(61) Lebedeva, N. P.; Koper, M. T. M.; Herrero, E.; Feliu, J. M.; van Santen, R. A. *J. Electroanal. Chem.* **2000**, *487* (1), 37−44.
(62) Chen, Q.-S.; Vidal-Iglesias, F. J.; Solla-Gullon, J.; Sun, S.-G.; Feliu, J. M. *Chem. Sci.* **2012**, *3* (1), 136−147.
(63) Farias, M. J. S.; Tanaka, A. A.; Tremiliosi, G.; Feliu, J. M. *Electrochem. Commun.* **2011**, *13* (4), 338−341.
(64) Chen, Q. S.; Feliu, J. M.; Berna, A.; Climent, V.; Sun, S. G. *Electrochim. Acta* **2011**, *56* (17), 5993−6000.
(65) Lebedeva, N. P.; Koper, M. T. M.; Feliu, J. M.; van Santen, R. A. *J. Phys. Chem. B* **2002**, *106* (50), 12938−12947.
(66) Angelucci, C. A.; Herrero, E.; Feliu, J. M. *J. Phys. Chem. C* **2010**, *114* (33), 14154−14163.
(67) Lebedeva, N. P.; Rodes, A.; Feliu, J. M.; Koper, M. T. M.; van Santen, R. A. *J. Phys. Chem. B* **2002**, *106* (38), 9863−9872.
(68) Herrero, E.; Feliu, J. M.; Wieckowski, A.; Clavilier, J. *Surf. Sci.* **1995**, *325* (2), 131−138.
(69) Feliu, J. M.; Orts, J. M.; Femandez-Vega, A.; Aldaz, A.; Clavilier, J. *J. Electroanal. Chem.* **1990**, *296* (1), 191−201.
(70) Orts, J. M.; Louis, E.; Sander, L. M.; Feliu, J. M.; Aldaz, A.; Clavilier, J. *Surf. Sci.* **1998**, *416* (3), 371−383.
(71) Chen, Q.-S.; Berna, A.; Climent, V.; Sun, S.-G.; Feliu, J. M. *Phys. Chem. Chem. Phys.* **2010**, *12*, 11407.
(72) Wasileski, S. A.; Koper, M. T. M.; Weaver, M. J. *J. Phys. Chem. B* **2001**, *105* (17), 3518−3530.
(73) Koper, M. T. M.; Jansen, A. P. J.; van Santen, R. A.; Lukkien, J. J.; Hilbers, P. A. J. *J. Chem. Phys.* **1998**, *109* (14), 6051−6062.
(74) Shubina, T. E.; Hartnig, C.; Koper, M. T. M. *Phys. Chem. Chem. Phys.* **2004**, *6* (16), 4215−4221.
(75) Housmans, T. H. M.; Hermse, C. G. M.; Koper, M. T. M. *J. Electroanal. Chem.* **2007**, *607* (1), 69−82.
(76) Inkaew, P.; Korzeniewski, C. *Phys. Chem. Chem. Phys.* **2008**, *10*, 3655.
(77) Inkaew, P., Ph.D. Dissertation, Texas Tech University, 2008.
(78) Dunietz, B. D.; Markovic, N. M.; Ross, P. N.; Head-Gordon, M. *J. Phys. Chem. B* **2004**, *108* (28), 9888−9892.
(79) Saravanan, C.; Markovic, N. M.; Head-Gordon, M.; Ross, P. N. *J. Chem. Phys.* **2001**, *114* (14), 6404−6412.

(80) Lucas, C. A.; Markovic, N. M.; Grgur, B. N.; Ross, P. N. *Surf. Sci.* **2000**, *448* (2−3), 65−76.
(81) Strmcnik, D. S.; Tripkovic, D. V.; van der Vliet, D.; Chang, K. C.; Komanicky, V.; You, H.; Karapetrov, G.; Greeley, J.; Stamenkovic, V. R.; Markovic, N. M. *J. Am. Chem. Soc.* **2008**, *130* (46), 15332−15339.
(82) Lucas, C. A.; Markovic, N. M.; Ross, P. N. *Surf. Sci.* **1999**, *425* (1), L381−L386.
(83) Arenz, M.; Mayrhofer, K. J. J.; Stamenkovic, V.; Blizanac, B. B.; Tomoyuki, T.; Ross, P. N.; Markovic, N. M. *J. Am. Chem. Soc.* **2005**, *127* (18), 6819−6829.
(84) Markovic, N. M.; Lucas, C. A.; Rodes, A.; Stamenkovic, V.; Ross, P. N. *Surf. Sci.* **2002**, *499* (2−3), L149−L158.
(85) Mayrhofer, K. J. J.; Blizanac, B. B.; Arenz, M.; Stamenkovic, V. R.; Ross, P. N.; Markovic, N. M. *J. Phys. Chem. B* **2005**, *109* (30), 14433−14440.
(86) Markovic, N. M.; Ross, P. N. *Electrochim. Acta* **2000**, *45* (25−26), 4101−4115.
(87) Mayrhofer, K. J. J.; Arenz, M.; Blizanac, B. B.; Stamenkovic, V.; Ross, P. N.; Markovic, N. M. *Electrochim. Acta* **2005**, *50* (25−26), 5144−5154.
(88) Petukhov, A. V.; Akemann, W.; Friedrich, K. A.; Stimming, U. *Surf. Sci.* **1998**, *402*−*404*, 182−186.
(89) Friedrich, K. A.; Geyzers, K. P.; Dickinson, A. J.; Stimming, U. *J. Electroanal. Chem.* **2002**, *524*−*525*, 261−272.
(90) Friedrich, K. A.; Henglein, F.; Stimming, U.; Unkauf, W. *Electrochim. Acta* **2000**, *45* (20), 3283−3293.
(91) Maillard, F.; Savinova, E. R.; Stimming, U. *J. Electroanal. Chem.* **2007**, *599* (2), 221−232.
(92) Yan, Y.-G.; Peng, B.; Yang, Y.-Y.; Cai, W.-B.; Bund, A.; Stimming, U. *J. Phys. Chem. C* **2011**, *115* (13), 5584−5592.
(93) Yan, Y.-G.; Yang, Y.-Y.; Peng, B.; Malkhandi, S.; Bund, A.; Stimming, U.; Cai, W.-B. *J. Phys. Chem. C* **2011**, *115* (33), 16378−16388.
(94) Batista, E. A.; Iwasita, T.; Vielstich, W. *J. Phys. Chem. B* **2004**, *108* (38), 14216−14222.
(95) Giz, M. J.; Batista, E. A.; Vielstich, W.; Iwasita, T. *Electrochem. Commun.* **2007**, *9* (5), 1083−1085.
(96) Wieckowski, A.; Rubel, M.; Gutiérrez, C. *J. Electroanal. Chem.* **1995**, *382* (1−2), 97−101.
(97) Dabo, I.; Wieckowski, A.; Marzari, N. *J. Am. Chem. Soc.* **2007**, *129* (36), 11045−11052.
(98) Tong, Y. Y.; Rice, C.; Wieckowski, A.; Oldfield, E. *J. Am. Chem. Soc.* **2000**, *122* (6), 1123−1129.
(99) Park, S.; Tong, Y. Y.; Wieckowski, A.; Weaver, M. J. *Langmuir* **2002**, *18* (8), 3233−3240.
(100) Rice, C.; Tong, Y. Y.; Oldfield, E.; Wieckowski, A.; Hahn, F.; Gloaguen, F.; Leger, J. M.; Lamy, C. *J. Phys. Chem. B* **2000**, *104* (24), 5803−5807.
(101) Liu, R.; Iddir, H.; Fan, Q.; Hou, G.; Bo, A.; Ley, K. L.; Smotkin, E. S.; Sung, Y.-E.; Kim, H.; Thomas, S.; Wieckowski, A. *J. Phys. Chem. B* **2000**, *104* (15), 3518−3531.
(102) Yoshimi, K.; Song, M.-B.; Song; Ito, M. *Surf. Sci.* **1996**, *368* (1−3), 389−395.
(103) Samjeske, G.; Komatsu, K.-i.; Osawa, M. *J. Phys. Chem. C* **2009**, *113* (23), 10222−10228.
(104) Yamakata, A.; Osawa, M. *J. Phys. Chem. C* **2008**, *112* (30), 11427−11432.
(105) Yan, Li, Q.-X.; Huo, S.-J.; Ma, M.; Cai, W.-B.; Osawa, M. *J. Phys. Chem. B* **2005**, *109* (16), 7900−7906.
(106) Zhu, Y.; Uchida, H.; Watanabe, M. *Langmuir* **1999**, *15* (25), 8757−8764.
(107) Sato, T.; Kunimatsu, K.; Uchida, H.; Watanabe, M. *Electrochim. Acta* **2007**, *53* (3), 1265−1278.
(108) Kunimatsu, K.; Sato, T.; Uchida, H.; Watanabe, M. *Electrochim. Acta* **2008**, *53* (21), 6104−6110.
(109) Watanabe, M.; Sato, T.; Kunimatsu, K.; Uchida, H. *Electrochim. Acta* **2008**, *53* (23), 6928−6937.
(110) Kunimatsu, K.; Sato, T.; Uchida, H.; Watanabe, M. *Langmuir* **2008**, *24* (7), 3590−3601.
(111) Hanawa, H.; Kunimatsu, K.; Uchida, H.; Watanabe, M. *Electrochim. Acta* **2009**, *54* (26), 6276−6285.
(112) Igarashi, H.; Fujino, T.; Watanabe, M. *J. Electroanal. Chem.* **1995**, *391*, 119−123.
(113) van Muylder, J.; Pourbaix, M.. Carbon. In *Atlas of Electrochemical Equilibria in Aqueous Solutions*, Pourbaix, M., Ed.; Pergamon Press: Oxford, 1966; Section 17.1, pp 449−457.
(114) Atkins, P. W. *Physical Chemistry*, 6th ed.; Oxford University Press: Oxford, 1998.
(115) Mayrhofer, K. J. J.; Hanzlik, M.; Arenz, M. *Electrochim. Acta* **2009**, *54* (22), 5018−5022.
(116) Jiang, T.; Mowbray, D. J.; Dobrin, S.; Falsig, H.; Hvolbæk, B.; Bligaard, T.; Nørskov, J. K. *J. Phys. Chem. C* **2009**, *113* (24), 10548−10553.
(117) Somorjai, G.; Li, Y. *Introduction to Surface Chemistry and Catalysis*, 2nd ed.; John Wiley & Sons: Hoboken, NJ, 2010.
(118) Furuya, N.; Koide, S. *Surf. Sci.* **1989**, *220* (1), 18−28.
(119) Gomez-Marin, A. M.; Feliu, J. M. *Electrochim. Acta* **2012**, *82* (Nov 1), 558−569.
(120) Delley, B. *J. Chem. Phys.* **1990**, *92* (1), 508−517.
(121) Delley, B. *J. Chem. Phys.* **2000**, *113* (18), 7756−7764.
(122) Delley, B. *Phys. Rev. B* **2002**, *66* (15), 155125.
(123) Perdew, J. P.; Burke, K.; Ernzerhof, M. *Phys. Rev. Lett.* **1997**, *78*, 1396.
(124) Orita, H.; Itoh, N.; Inada, Y. *Surf. Sci.* **2004**, *571* (1−3), 161−172.
(125) Tränkenschuch, B.; Papp, C.; Fuhrmann, T.; Denecke, R.; Steinrück, H.-P. *Surf. Sci.* **2007**, *601*, 1108−1117.
(126) Yamagishi, S.; Fujimoto, T.; Inada, Y.; Orita, H. *J. Phys. Chem. B* **2005**, *109* (18), 8899−8908.
(127) Marković, N. M.; Grgur, B. N.; Lucas, C. A.; Ross, P. N. *J. Phys. Chem. B* **1999**, *103* (44), 487−495.
(128) Markovic, N. M.; Ross, P. N. *Surf. Sci. Rep.* **2002**, *45*, 117−229.
(129) Villegas, I.; Weaver, M. J. *J. Chem. Phys.* **1994**, *101* (2), 1648−1660.
(130) Tao, F.; Dag, S.; Wang, L.-W.; Liu, Z.; Butcher, D. R.; Bluhm, H.; Salmeron, M.; Somorjai, G. A. *Science* **2010**, *327* (5967), 850−853.
(131) Björling, A.; Herrero, E.; Feliu, J. M. *J. Phys. Chem. C* **2011**, *115*, 15509−15515.
(132) Fang, Y.-H.; Liu, Z.-P. *J. Phys. Chem. C* **2009**, *113*, 9765−9772.
(133) Bandlow, J.; Kaghazchi, P.; Jacob, T.; Papp, C.; Tränkenschuh, B.; Streber, R.; Lorenz, M. P. A.; Fuhrmann, T.; Denecke, R.; Steinrück, H.-P. *Phys. Rev. B* **2011**, *83*, 174107−1−5.
(134) van Muylder, J.; de Zoubov, N.; Pourbaix, M.. Platinum. In *Atlas of Electrochemical Equilibria in Aqueous Solution*; Pourbaix, M., Ed.; Pergamon Press: Oxford, 1966; Section 13.6, pp 278−283.
(135) Matsumoto, M.; Miyazaki, T.; Imai, H. *J. Phys. Chem. C* **2011**, *115*, 11163−11169.
(136) Deeth, R. J.; Elding, L. I. *Inorg. Chem.* **1996**, *35*, 5019−5026.
(137) Hwang, G.; Bodenbinder, M.; Willner, H.; Aubke, F. *Inorg. Chem.* **1993**, *32*, 4667−4669.
(138) Frank, M.; Kühnemuth, R.; Bäumer, M.; Freund, H.-J. *Surf. Sci.* **2000**, *454*−*456*, 968−973.
(139) Orita, H.; Inada, Y. *J. Phys. Chem. B* **2005**, *109* (47), 22469−22475.
(140) Santana, J. A.; Ishikawa, Y. *Chem. Phys. Lett.* **2009**, *478* (4−6), 110−114.
(141) Santana, J. A.; Ishikawa, Y. *Electrochim. Acta* **2010**, *56* (2), 945−952.
(142) Orita, H.; Itoh, N.; Inada, Y. *Chem. Phys. Lett.* **2004**, *384* (4−6), 271−276.
(143) Iwasita, T.; Xia, X. *J. Electroanal. Chem.* **1996**, *411* (1−2), 95−102.
(144) Ishikawa, Y.; Mateo, J. J.; Tryk, D. A.; Cabrera, C. R. *J. Electroanal. Chem.* **2007**, *607* (1−2), 37−46.
(145) Mateo, J. J.; Tryk, D. A.; Cabrera, C. R.; Ishikawa, Y. *Mol. Simul.* **2008**, *34* (10−15), 1065−1072.

(146) Santana, J. A.; Mateo, J. J.; Ishikawa, Y. *J. Phys. Chem. C* **2010**, *114* (11), 4995−5002.
(147) Xu, J.; Henriksen, P.; Yates, J. T. *J. Chem. Phys.* **1992**, *97* (7), 5250−5252.
(148) Xu, J.; Yates, J. T. *J. Chem. Phys.* **1993**, *99* (1), 725−732.
(149) We also note that the orientation change of water molecules corresponds closely to the potential of maximum entropy (pme), which has been proposed to correspond closely to both the potential of zero total charge (pztc) and the potential of zero free charge (pzfc) for Pt(111), with a best value of 0.37 V vs RHE, based on recent work of Garcia-Araez et al. on Pt(111) in 0.1 M $HClO_4$: Garcia-Araez, N.; Climent, V.; Feliu, J. *J. Phys. Chem. C* **2009**, *113* (21), 9290−9304. There also remains an unresolved issue in the literature regarding the effective surface potential in ultrahigh vacuum vs that in electrolyte solution for CO-covered Pt(111): Villegas, I.; Weaver, M. J. *J. Phys. Chem. B* **1997**, *101* (49), 10166−10177. Although this issue is certainly important and will be treated separately elsewhere, for the purposes of the present work, we believe that it does not pose a fundamental impediment to the comparison of experimental and theoretical results.